International Journal of Thermal Sciences 58 (2012) 61–69

Contents lists available at SciVerse ScienceDirect

International Journal of Thermal Sciences

journal homepage: www.elsevier.com/locate/ijts

Heat transfer enhancement in a straight channel via a rotationally oscillating adiabatic cylinder

Ali Beskok [a,*], Mehrdad Raisee [c], Bayram Celik [b], Bedri Yagiz [a], Mohsen Cheraghi [c]

[a] Old Dominion University, Institute of Micro and Nanotechnology, Norfolk, VA 23523, USA
[b] Istanbul Technical University, Aerospace Engineering Department, Istanbul, Turkey
[c] University of Tehran, School of Mechanical Engineering, Tehran, Iran

ARTICLE INFO

Article history:
Received 6 January 2012
Received in revised form
19 March 2012
Accepted 20 March 2012
Available online 24 April 2012

Keywords:
Vortex dynamics
Internal flow
Lock-in regime
Time periodic flow and heat transfer

ABSTRACT

Heat convection from the uniformly heated walls of a straight channel in presence of a rotationally oscillating cylinder (ROC) is simulated at $Re = 100$. Heat transfer enhancement due to vortex shedding from the ROC is investigated. Systematic studies are performed to explore the rotation angle and frequency influences on heat transfer by varying the latter in range of the lock-in regime and the former from 0 to $2\pi/3$. All simulation results are based on the numerical solutions of two-dimensional, unsteady, incompressible Navier–Stokes and energy equations using an h/p type finite element algorithm. Considering time periodicity of the resulting flow and temperature fields, time averaged wall Nusselt number is reported to quantify the heat transfer enhancement for $Pr = 0.1$, 1.0, 5.0 and 10.0 fluids. Performance analyses of the ROC device based on its total power consumption and heat transfer enhancement are also presented.

1. Introduction

Convective heat transfer can be enhanced by geometric modifications of the boundaries or by oscillations of solid structures at critical locations within the flow system. Casting artificial roughness or placing obstacles on the system boundaries are examples of the former application [1]. Oscillating structures and actuators can induce flow kinematics that enhances local heat transfer by thinning the thermal boundary layers. This approach is specifically effective for laminar flow heat transfer enhancement in meso-scale channels, where the flow kinematics can be actively controlled using micro-electro-mechanical-systems (MEMS).

Motivated by the potential applications of MEMS actuators, Celik et al. have conducted a numerical study to investigate the kinematics of flow past a transversely oscillating circular cylinder confined in a straight channel [2]. Their study was conducted at $Re = 100$, where the inertial effects were large enough to induce time periodic two-dimensional flow with Karman vortex street behind the cylinder. They performed a series of simulations at a wide range of cylinder oscillation frequencies, and determined the boundaries of the lock-in regime, where the vortex shedding and cylinder oscillations are synchronized. Flow kinematics resulting from the interactions of vortices shed from the cylinder with the wall shear layers was also described. Their investigations on flow kinematics led to two distinct studies that focused on the influences of vortex dynamics on mixing and heat transfer [3,4]. Although heat transfer from a transversely oscillating heated structure has been studied before [5–7], investigations on channel heat transfer enhancement due to an oscillating adiabatic structure are rather limited [4,8,9]. Celik et al. utilized the vortex shedding mechanism from a transversely oscillating adiabatic circular cylinder to enhance heat convection from uniformly heated channel walls [4]. Their study systematically assessed the effects of the oscillation frequency on heat transfer at $Re = 100$ by varying the excitation frequency from 75% to 125% of the natural vortex shedding frequency. Cylinder oscillations at the lowest lock-in frequency gave the best results due to high intensity vortex generation closer to the channel walls [4].

Transverse oscillations of a body within a channel have several limitations. First, the amplitude of oscillations must be small to avoid contact between the oscillating body and channel walls. Second, design, fabrication and control of such an actuator could be rather challenging. Alternatively, one can induce rotational oscillations on the body, which does not limit the amplitude of rotation. In addition, the design, fabrication and operation of such an actuator would be easier. A limited number of studies on flow past a rotationally oscillating cylinder are available in the literature.

* Corresponding author. Tel.: +1 757 683 6818.
E-mail address: abeskok@odu.edu (A. Beskok).

1290-0729/$ – see front matter © 2012 Elsevier Masson SAS. All rights reserved.
doi:10.1016/j.ijthermalsci.2012.03.012

Nomenclature

A	maximum oscillation amplitude
D	cylinder diameter
D_h	hydraulic diameter
f_o	natural vortex shedding frequency
f_e	cylinder excitation frequency
F	normalized excitation frequency $= f_e/f_o$
L	channel length
H	channel height
HP	heat performance
k	thermal conductivity
M	instantaneous torque on the cylinder
NOC	non-oscillating cylinder
Nu	Nusselt number
Nu_s	average Nusselt number in a straight channel
$\overline{Nu}$	time averaged Nusselt number
$\overline{Nu}_{ave}$	spatial average of $\overline{Nu}$
Pe	Peclet number
Pr	Prandtl number
Po	normalized power ratio
q	normalized heat flux
Re	Reynolds number
ROC	rotationally oscillating cylinder
St	Strouhal number $= f_oD/U$
t	time
T	temperature
T_b	bulk temperature
T_w	wall temperature
TOC	transversely oscillating cylinder
U	characteristic velocity
u,v	velocity components
$\mathbf{u}$	velocity vector
x, y	distances from the cylinder center
$\dot{W}$	power needed to oscillate the cylinder

Greek

Θ_{max}	the maximum rotation angle
τ	vortex shedding period

Subscripts

$'$	dimensional quantities
s	straight channel
ave	spatial average
ω	angular velocity $= 2\pi/\tau$

Based on the numerical and experimental results, presence of a lock-in state in such flows is reported by Okajima et al. [10], while periodic vortex shedding from a rotationally oscillating cylinder is experimentally visualized in [11]. Using numerical studies, Wu et al. showed that the rotational oscillation could modify the wake structure as observed in the case of transverse oscillations [12]. Mahfouz and Badr have shown through numerical simulations that the primary lock-in regime is widened as the maximum oscillation angle is increased [13]. This finding was confirmed experimentally in [14].

The *objective* of the present study is to enhance heat transfer from the walls of a straight channel by utilizing the vortex shedding mechanism from an adiabatic circular cylinder subjected to forced rotational oscillations. Influences of vortex dynamics on heat transfer from the channel walls subjected to constant heat flux are investigated systematically at $Re = 100$ using a wide range of oscillation amplitudes and frequency values, and for various Prandtl number fluids corresponding to typical gases like air and liquids like water and refrigerants. Using a similar channel-cylinder configuration, numerical predictions of the rotationally oscillating cylinder are compared with the results of the transversely oscillating cylinder, previously presented in [4].

This paper is organized as follows: the governing equations and details of the utilized numerical algorithm are presented in Section 2 along with the problem definition, geometry and the boundary conditions. Kinematics of the flow, time averaged Nusselt number concept used for quantification of heat transfer, and system's behavior under various frequency oscillation amplitudes, and for different Prandtl number fluids are given in the Results and Discussions section. In Section 4, we present the conclusion of this study.

2. Governing equations and the problem definition

The simulations presented here are based on the numerical solutions of two-dimensional unsteady incompressible Navier–Stokes and energy equations given in the following non-dimensional form:

$$\frac{\partial u}{\partial t} + \mathbf{u}\cdot\nabla\mathbf{u} = -\nabla p + \frac{1}{\mathrm{Re}}\nabla^2\mathbf{u}, \tag{1}$$

where the velocity vector $\boldsymbol{u}$ satisfies the continuity equation written as

$$\nabla\cdot\mathbf{u} = 0. \tag{2}$$

The energy equation in non-dimensional form is given as follows

$$\frac{\partial T}{\partial t} + u\cdot\nabla T = \frac{1}{p_e}\nabla^2 T. \tag{3}$$

non-dimensionalization in equations (1)–(3) is based on the cylinder diameter, D, and the channel averaged velocity, U. In equation (3), the non-dimensional temperature, T, is defined as $T = (T' - T'_{b\,in})/\Delta T'_b$, where $T\prime$ is the temperature, $T'_{b\,in}$ is the inlet bulk temperature and $\Delta T'_b$ is the bulk temperature difference between the outlet and inlet of the channel. Normalized heat flux is defined by $q = q'D/k\Delta T'_b$, where q' is the heat flux and k is the thermal conductivity.

The Reynolds number based on the cylinder diameter and channel averaged velocity, is kept constant at $Re = 100$ in all simulations, while Prandtl number is varied between 0.1 and 10.0 In this study, an h/p type finite element algorithm is used in the solutions of equations (1)–(3). The algorithm utilizes a third-order accurate temporal discretization based on an operator splitting scheme [15]. The spatial discretization is based on high-order modal expansions on quadrilateral and triangular elements, and exhibits exponential reduction in error with increased modes. This feature of the algorithm, also called spectral convergence, allows us to increase the spatial accuracy on a computational domain by simply increasing the modal expansion order of the elements (p type refinement) without changing the element sizes and numbers [16]. More detail on the algorithm and the code validation can be found in [17].

Fig. 1 shows the computational domain, where the circular cylinder with diameter D is located at 1.5D and 4D away from

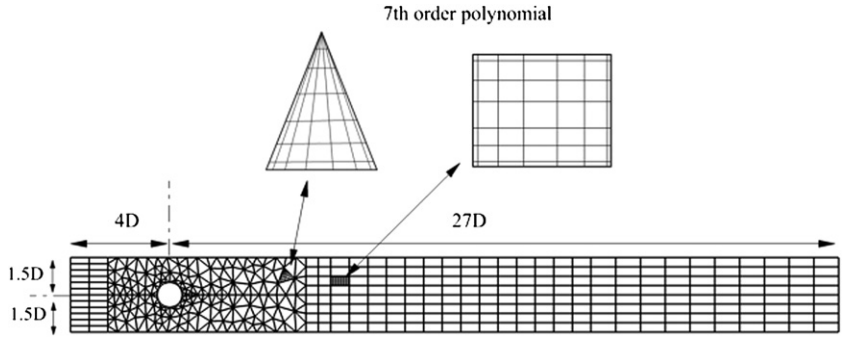

Fig. 1. The computational domain and its spectral element discretization. Close-up views of the triangular and quadrilateral elements show the quadrature points used for 7th order discretization.

channel walls and the domain inlet, respectively. A fully developed flow at constant temperature $T = 0.0$ enters the channel from left. The velocity profile is parabolic at the inlet, resulting in maximum channel velocity of 1.5U. The channel is 31D in length and 3D in height. The channel walls are subjected to constant heat flux of $q = 1.0$, while the cylinder is adiabatic. We imposed no-slip boundary conditions on the channel and cylinder walls, and set zero-Neumann boundary conditions for both velocity and temperature at the outlet. Fig. 1 also illustrates the spectral element discretization of the computational domain, which consists of 314 triangular and 232 quadrilateral elements. The figure shows the quadrature points used for 7th order discretizations on triangular and quadrilateral elements. Our simulations utilized 7th order expansions for $Pr = 1$, and $Pr = 5$ cases, and 9th order expansion for $Pr = 10$ cases to achieve grid independent results, as previously shown in [4].

The adiabatic circular cylinder is subjected to forced rotational oscillations that result in time periodic tangential velocity on the cylinder according to following formula:

$$V_\theta = \Theta_{\max} * \pi f_e * D * \sin(2\pi f_e t), \tag{4}$$

where f_e and $\Theta_{\max}$ are the excitation frequency and the maximum rotation angle, respectively. In order to determine the *natural vortex shedding frequency*, f_o, of the system depicted in Fig. 1, we tracked the history of the force exerted on the stationary cylinder, and obtained $St = 0.36$ [2,4]. Then we performed a series of simulations at various rotational oscillation frequencies. The results are presented as a function of the normalized excitation frequency $F = f_e/f_o$, which was varied systematically within $0.5 \le F \le 1.5$ range. We have also varied the maximum rotation angle within the range of $0 \le \Theta_{\max} \le 2/3\pi$, where Θ is defined using polar coordinates at the center of the cylinder.

In order to verify that the flow remains two-dimensional within the parametric ranges used in this study, three-dimensional simulations at $Re = 100$ for $F = 1$ and $\Theta_{\max} = 2/3\pi$ are performed in a similar domain that is 20D wide. Symmetry boundary conditions were imposed on the side surfaces. Long time integration of this three-dimensional case verified that the flow remains two-dimensional. For the parametric ranges studied here, flows with $0.75 \le F \le 1.25$ are in the lock-in regime, where the vortex shedding mechanism synchronizes with the cylinder rotation and yields time periodic temperature and velocity fields. We observed sub-harmonic synchronization for $F = 0.5$, and coalescence of the vortices in the formation region (the distance from the cylinder to the start of the Karman vortex shedding) for $F > 1.25$, which are similar behaviors to our observations for transversely oscillating cylinder [2].

3. Results and discussions

Compared with an external flow past a circular cylinder, the flow around a circular cylinder confined in a channel is quite complicated because of interaction of the vortices shed from the cylinder with the shear layers formed on the channel walls [2,18]. In Fig. 2, we show the vorticity and temperature contours in the channel for the stationary (NOC), transversely oscillating (TOC), and rotationally oscillating (ROC) cylinders at $Re = 100$ and $Pr = 1.00$. All contours are shown at an instant when the cylinder is at its level position (i.e., $y = 0$ and $\Theta = 0$ for the TOC and ROC cases, respectively). At the instant shown in the figure, the TOC is moving upwards and ROC is rotating in counter-clockwise direction. The normalized cylinder excitation frequency, F, is equal to 1.00 for both ROC and TOC cases, while the transverse oscillation amplitude is $A = 0.4D$, and the maximum rotation angle is $\Theta_{\max} = \pi/4$. These cases correspond to approximately equal magnitudes of transverse and tangential velocities for the TOC and ROC cases, respectively. Despite the differences between the motions of the two cases, the resulting vorticity fields show striking similarities in the vortex shedding region. Braided downstream temperature contours and corrugated thermal boundary layer structures are observed in both types of oscillations. However there are subtle differences in the formation region ($4 \le x/D \le 9$). The ROC tends to wrap the positive and negative shear layers around the cylinder as the maximum rotation angle is increased.

3.1. Quantification of heat transfer

We calculate the instantaneous Nusselt number variation along the channel walls using:

$$Nu(x,t) = \frac{q' D_h}{k(T'_{\text{wall}} - T'_b)} \tag{5}$$

where T_b is the bulk temperature defined as:

$$T_b(x,t) = \int_0^H uTdy \Big/ \int_0^H udy. \tag{6}$$

Due to the time periodic nature of the flow and temperature field, instantaneous wall Nusselt number calculated from equation (5) is also periodic. However, there is a phase lag between the upper and lower walls' Nu values induced by oscillatory motion of the cylinder, as previously shown in [4]. Integrating the local Nusselt number, $Nu(x,t)$, over the vortex shedding period gives time averaged Nusselt number:

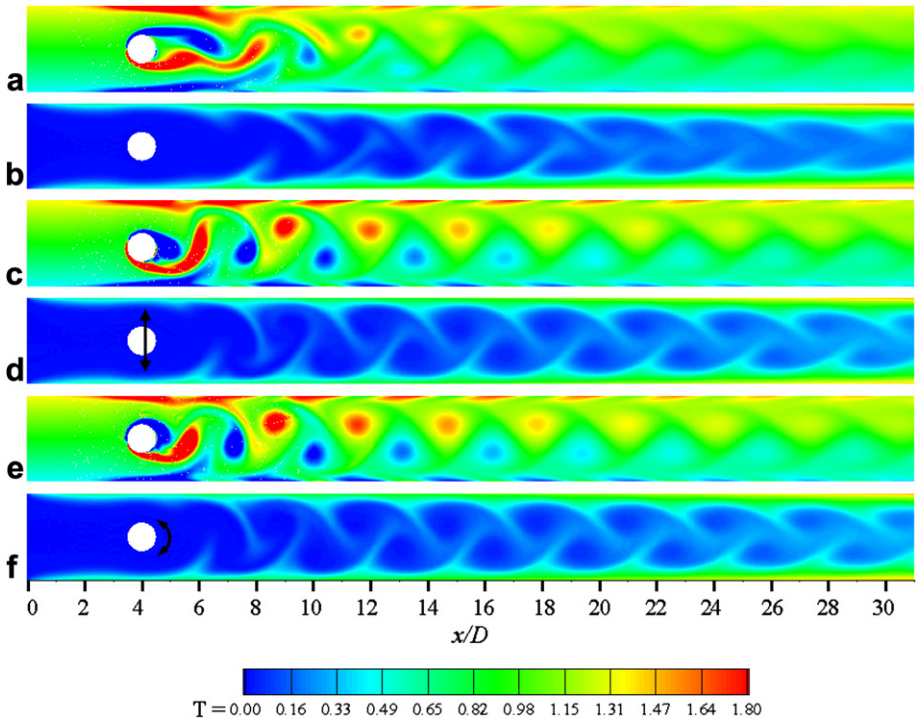

Fig. 2. Vorticity and temperature contours at $Re = 100$ and $Pr = 1.0$ for the stationary cylinder (a) and (b); for transversely oscillating cylinder with $F = 1.00$ and $A = 0.4D$ (c) and (d); for rotationally oscillating cylinder with $F = 1.00$ and $\Theta_{max} = \pi/4$ (e) and (f).

$$\overline{Nu}(x) = \frac{1}{\tau}\int_0^{\tau} Nu(x,t)dt. \tag{7}$$

In the following we investigate the influence of the cylinder excitation frequency and the rotary oscillation amplitude on heat transfer, and then examine the validity of these at various Prandtl numbers.

3.2. Effects of the excitation frequency

In Fig. 3 we show the variation of time averaged Nusselt number along the channel walls obtained at fixed rotary oscillation amplitude of $\Theta_{max} = \pi/4$ and F values ranging from 0.5 to 1.0 at $Pr = 1$. In addition, we also show the results for the straight channel (SC) without a cylinder, and non-oscillating cylinder (NOC) cases in the figure. For the straight channel case, the flow is steady and the time averaged and instantaneous Nusselt numbers are the same. After a monotonic decrease in the stream wise direction, the time averaged wall Nu for the straight channel case reaches the fully developed value of 8.23 [19].

Due to the presence of a non-oscillating cylinder in the channel (NOC), relatively higher stream wise velocities occur between the cylinder and the channel walls induced by the high blockage ratio (=1/3). The accelerated flow thins thermal boundary layers on the channel walls (see Fig. 2b,d and f) and thereby enhances heat transfer. This enhancement is evident from the time averaged wall Nusselt number shown in Fig. 3, where $\overline{Nu}$ gradually increases and reaches a peak at $x/D \approx 4.0$. However, this local enhancement disappears rapidly because of the thickening thermal boundary layers within the region extending from the cylinder to the end of formation region. As can be seen from the instantaneous vorticity contours in Fig. 2, shear layers from the cylinder curl up and extend toward the wall in the formation region ($x/D \leq 10$). If the influence of the cylinder shear layer on the channel wall is strong enough, the wall shear layer next to it also detaches from the wall and curls up. The detached shear layer convects a stream that transports the hot fluid in the upstream shear layer away from the wall. Due to the periodic vortex shedding mechanism, an identical hot fluid stream occurs on the other wall half time period later. This roll up mechanism thickens the thermal boundary layer in the formation region and reduces heat transfer from the wall. After the formation region, the vortices shed from the cylinder roll up the wall shear layers and wrap around themselves. This mechanism convects hot fluid stream away from the wall and enables its interaction with the

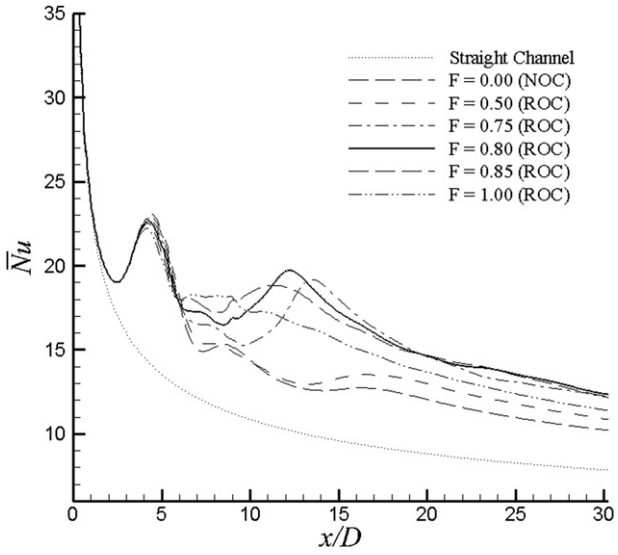

Fig. 3. Time averaged wall Nusselt number variation as a function of the oscillation frequency F. Simulations are performed for $\Theta_{max} = \pi/4$, $Pr = 1.0$ and $Re = 100$. Results for the straight channel and stationary cylinder (NOC) are also shown.

colder fluid in the channel, resulting in the braided temperature contours shown in Fig. 2.

Heat transfer enhancement due to the solid body rotation of vortices results in a second peak in $\overline{Nu}$ after the formation region. As can be seen from Fig. 3, the vortex shedding from the cylinder enhances heat transfer considerably (NOC), and this enhancement is further increased by the forced rotational oscillations of the cylinder (ROC). For all excitation frequencies studied here, the ROC cases exhibit better heat transfer than the NOC case. Two distinct peaks in time averaged Nusselt number are observed for the ROC cases up to the excitation frequency of 0.90. For higher frequencies, the second peak emerging after the formation region disappears due to the diminishing influence of vortex dynamics on heat transfer, as previously shown for the TOC cases [4].

In order to summarize our observations for higher *Pr* fluids, we present in Table 1 the locations and magnitudes of the two distinct $\overline{Nu}$ peaks of the simulated cases for $Pr = 5$ fluid. We also give the spatial averages of $\overline{Nu}$ along the channel wall; $\overline{Nu}_{ave}$. According to this table, the frequency values of $F = 0.80$ results in the highest $\overline{Nu}_{ave}$. While the magnitude of the first peak and its distance from the cylinder center continuously decreases with increasing frequency, the magnitude of the second peak increases up to $F = 0.80$, and it disappears after $F = 0.90$. It is noted that the second peak has a significant contribution to $\overline{Nu}_{ave}$, which enhances heat transfer up to 24% percent relative to the TOC case with $F = 0.75$ and $A = 0.4D$ studied in [4].

3.3. Effects of the oscillation amplitude

In order to investigate the influence of the rotary oscillation amplitude on heat transfer, we present the time averaged wall *Nu* variations for $\Theta_{max} = \pi/6$, $\pi/3$, $\pi/2$ and $2\pi/3$ in Fig. 4 obtained for $Pr = 1.0$ and $F = 0.80$. The corresponding vorticity and temperature contours are shown in Fig. 5. As can be seen from Fig. 4, the *Nu* variations of the considered cases are almost identical up to $x/D = 5.0$. Although a rapid reduction in *Nu* is observed for the NOC case, this adverse behavior diminishes with increased oscillation amplitude, resulting in better heat transfer performance. Observations from Fig. 5 show that the length of the vortex formation region is reduced with increased oscillation amplitude. In addition, vortex intensity of the free shear layers around the cylinder and their interactions with the wall share layers also increases; sustaining reasonably high *Nu* values in the formation region ($x/D \leq 9$) with increased oscillation amplitude. As can be seen in Fig. 4, *Nu* for the $\Theta_{max} = 2\pi/3$ case has a second maxima around $x/D = 7$ in the formation region, while $\Theta_{max} = \pi/2$ and $\pi/3$ cases exhibit a similar second peak at $x/D = 8$ and 9, respectively. The third maxima in $\overline{Nu}$ occur in the vortex shedding region, and its location

Table 1
The locations and magnitudes of the two $\overline{Nu}$ peaks, and its spatial average values for various excitation frequencies with a constant $\Theta_{max} = \pi/4$ at $Re = 100$ and $Pr = 5.0$. *Data is from [4].

F	The first peak		The second peak		$\overline{Nu}_{ave}$
	x/*D*	$\overline{Nu}$	*x*/*D*	$\overline{Nu}$	
0.50	4.29	46.31	17.81	27.52	28.83
0.75	4.23	45.73	13.52	34.63	31.58
0.80	**4.23**	**45.27**	**12.16**	**36.01**	**32.17**
0.85	4.22	44.87	11.34	34.69	31.91
0.90	4.22	44.66	NA	NA	31.31
0.95	4.22	44.27	NA	NA	30.50
1.00	4.16	44.16	NA	NA	29.60
1.25	4.16	44.01	NA	NA	26.22
0.75*	4.10	38.46	12.59	24.79	24.43

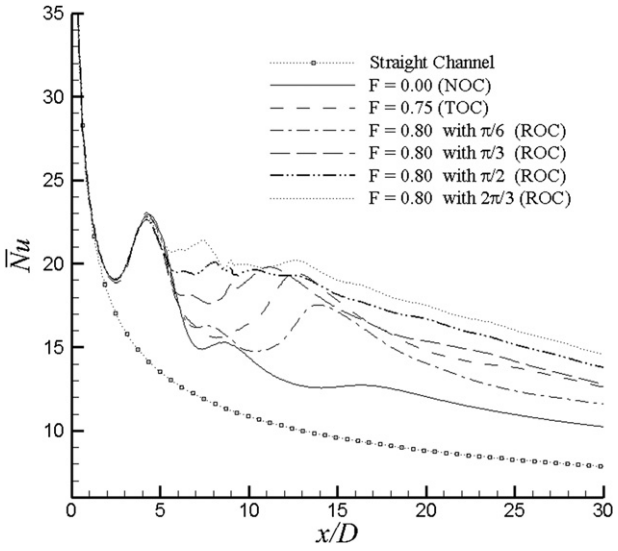

Fig. 4. Time averaged wall Nusselt number variation as a function of the rotational oscillation amplitude $\Theta_{max.}$ Simulations are performed for $F = 0.80$, $Pr = 1.0$ and $Re = 100$. Results for the straight channel, non-oscillating cylinder (NOC) and transversely oscillating channel (TOC) case at $F = 0.75$ are also shown.

and magnitude depends on the vortex spacing and strength. After this, the $\overline{Nu}$ is reduced along the channel.

3.4. Heat transfer enhancement for various fluids

Efficiency of a heat exchanger depends on the thermal properties of the working fluid, characterized by the Prandtl number. In order to understand heat transfer characteristics of the simulated systems, we performed simulations for $Pr = 0.1$, 1.0, 5.0 and 10.0 at the fixed kinematic condition of $Re = 100$, $F = 0.80$ and $\theta_{max} = 3\pi/2$. In Fig. 6, we present the time averaged wall *Nu* variations of the ROC cases, and include results from the TOC cases with $F = 0.75$ with $A = 0.4D$, which was promoted as the most efficient configuration in [4]. As can be seen from the figure, the rotational oscillation of the cylinder enhances heat transfer better than the transverse oscillations regardless of the Prandtl number. This can be attributed to the relatively higher magnitudes of the stream wise velocity generated by the rotational oscillation of the cylinder. In addition, differences in $\overline{Nu}$ variations between the ROC and TOC cases increase with increased *Pr*, with $Pr = 10$ cases resulting in the highest $\overline{Nu}$ values.

3.5. Performance analyses

This section examines the spatially averaged wall heat transfer, pressure drop and required mechanical power for creating fluid flow and cylinder oscillation to investigate how efficiently ROC can be used for channel cooling proposes. In Fig. 7, we show the spatially averaged Nusselt number ($\overline{Nu}_{ave}$) at Reynolds number of 100 for different fluids, various oscillation frequencies and amplitudes. The Nusselt number is normalized using the average Nusselt number of a straight channel (Nu_s). Since we are analyzing thermally developing flow at various *Pr* values, we obtain $Nu_s = 8.94$, 12.15, 19.04, and 23.76 for $Pr = 0.1$, 1, 5, and 10 cases, respectively. Consistent with the local *Nu* number distributions shown in Figs. 3, 4 and 6, considerable heat transfer enhancement is obtained due to the insertion of ROC in the channel. It is noted that the optimum heat transfer enhancement is around 60 percent and occurs for $Pr = 1$, $F = 0.8$, and $\Theta = 2\pi/3$. This could be related to the thermal

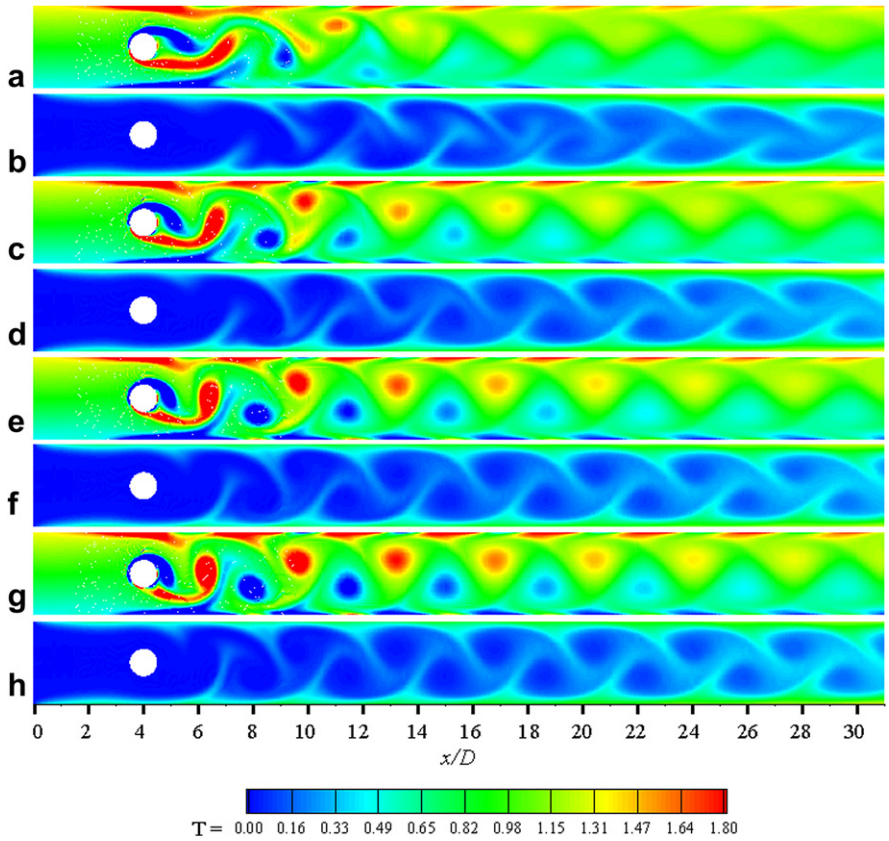

Fig. 5. The vorticity and temperature contours for $F = 0.80$, $Pr = 1.0$ and $Re = 100$ flows with $\Theta_{max} = \pi/6$ (a and b); $\Theta_{max} = \pi/3$ (c and d); $\Theta_{max} = \pi/2$ (e and f); $\Theta_{max} = 2\pi/3$ (g and h).

boundary layer thickness. For liquids with $Pr > 1$, the thermal boundary layer may be too thin to be effectively disturbed by mixing induced by the vortices shed from the cylinder. While for gases with $Pr < 1$, the thermal boundary layers cover most of the channel cross-section, and thus, vortices cannot effectively mix the hot and cold fluids in the channel.

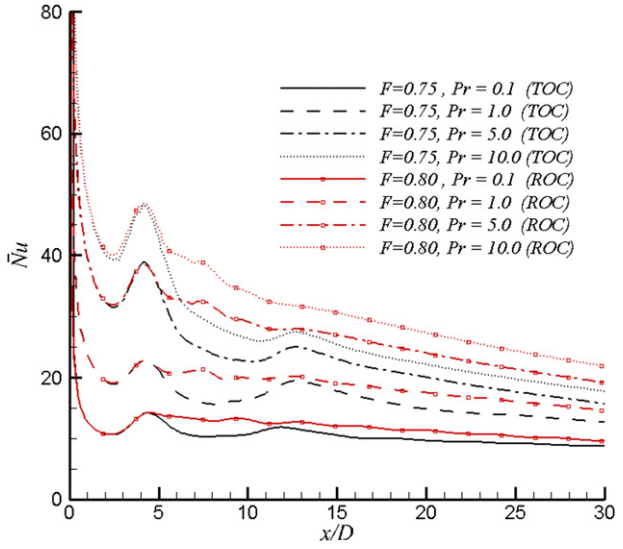

Fig. 6. Time averaged wall Nusselt number variation for different Prandtl number fluids obtained for ROC $Re = 100$ flows with $F = 0.80$ and $\Theta_{max} = 2\pi/3$, and their comparison with the TOC results with $F = 0.75$ and $A/D = 0.4$ presented in [4].

To calculate the mechanical power for oscillation of the rotating cylinder, we first calculated the instantaneous torque on the cylinder using:

$$M(t) = \frac{1}{4}\int_0^{2\pi} \mu \frac{\partial U(t)}{\partial n} D^2 d\Theta, \tag{8}$$

where n is the unit vector normal to the surface. Then the required mechanical power for one cycle of oscillation is obtained via:

$$\dot{W} = \frac{1}{\tau}\int_0^{\tau} M(t)\dot{\Theta}(t)dt. \tag{9}$$

Subsequently, we calculated the power ratio, Po, which is the ratio of the required power in ROC in a channel (i.e., sum of the oscillation and pumping powers) to the required pumping power of a plane channel flow (obtained by multiplying the pressure drop in the channel with the sustained volumetric flow rate). Fig. 8 shows the variation of this ratio (Po) at $Re = 100$, $0.5 \le F \le 1.25$ and $0 \le \Theta \le 2\pi/3$. This figure clearly shows increase in required power with increase in either the excitation frequency or oscillation amplitude. We note the four folds increase in mechanical power for $F = 0.8$ and $\Theta = 2\pi/3$ case, for which maximum heat transfer enhancement occurs. It is noted that for $\Theta_{max} > \pi/3$, the smallest value of Po parameter is obtained for excitation frequency of $F = 0.5$. Variation of power for cylinder oscillations and pumping power at $F = 0.8$ are provided in Table 2 for various oscillation amplitudes. While the power required for oscillating the cylinder increases with the increased oscillation amplitude, pumping power

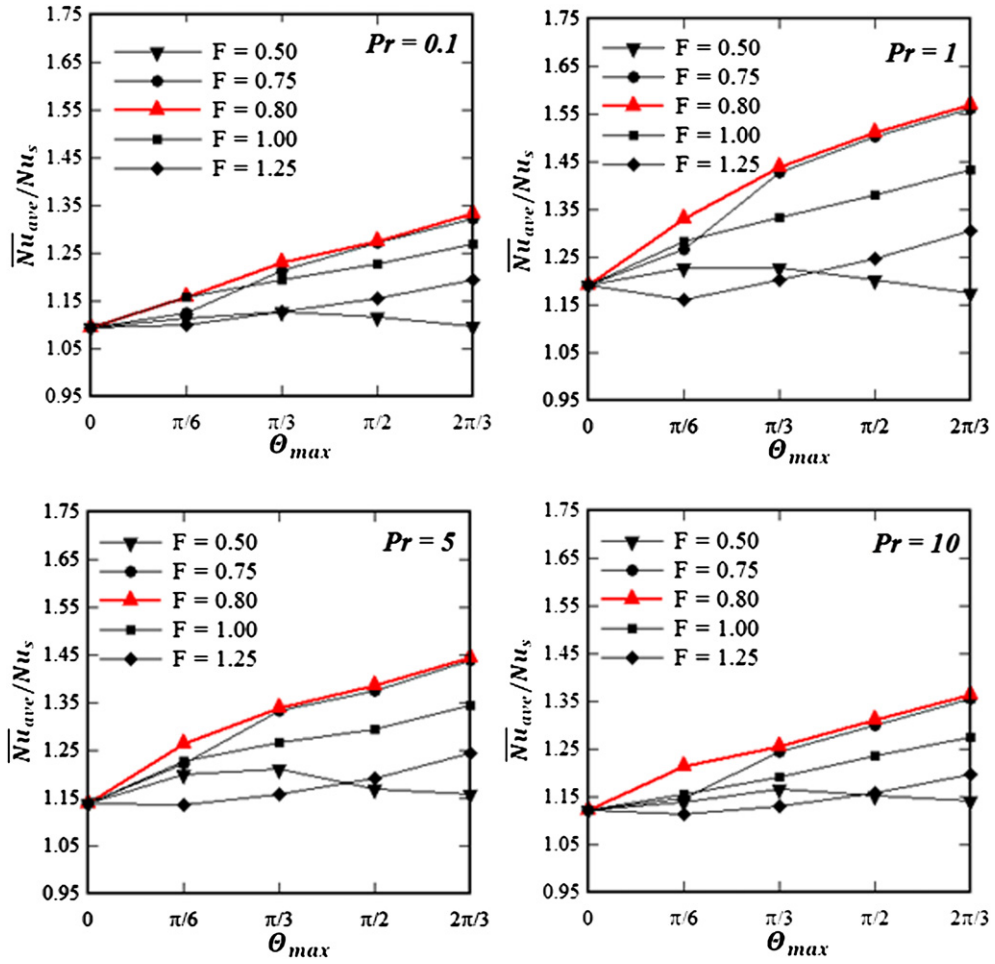

Fig. 7. Variation of the channel averaged Nusselt number of the ROC cases, normalized with the average Nusselt number of a straight channel (Nu_s) at various oscillation frequencies and amplitudes. Results are obtained for $Re = 100$ flow and various Pr values.

required to sustain the desired flow rate also increases with the increased oscillation amplitude. Results indicate that the main portion of the mechanical power is consumed to overcome the pressure losses (e.g. 96% at $F = 0.8$ and $\Theta = 2\pi/3$).

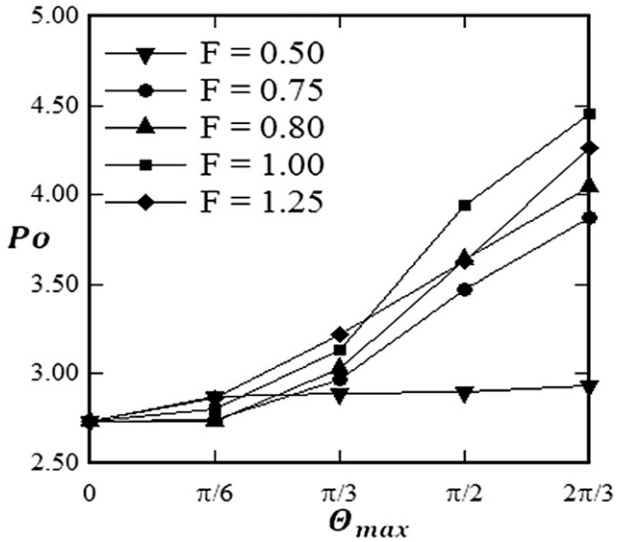

Fig. 8. Normalized power requirement of $Re = 100$ flow as a function of the oscillation frequency and amplitudes.

In order to study the usefulness of the insertion of the ROC for channel cooling proposes, heat transfer enhancements in Figs. 7and 8 must be compared with the corresponding values for the plane channel at *identical* pumping power requirements. For this propose the required power for ROC at each case is computed, and assumed to be used for generating flow through a plane channel. Using basic relations of laminar flow through plane channel the mean velocity for a given pumping power is obtained via [20]:

$$V^* = \sqrt{\dot{W}_T \times \frac{H}{12\mu L}}. \tag{10}$$

Using parabolic velocity profile with mean velocity of V^*, we calculated the average Nusselt number for plane channels (Nu_s^*) requiring pumping power *identical* to the ROC cases. Fig. 9

Table 2
Power requirement for $F = 0.8$ ROC flow at $Re = 100$. Power per unit channel width is normalized using $\rho U^3 D$.

Θ_{max}	Normalized mechanical power for cylinder oscillation	Normalized pumping power
0	0	3.37
π/6	1.16×10^{-1}	3.28
π/3	1.25×10^{-1}	3.62
π/2	1.56×10^{-1}	4.34
2π/3	1.81×10^{-1}	4.82

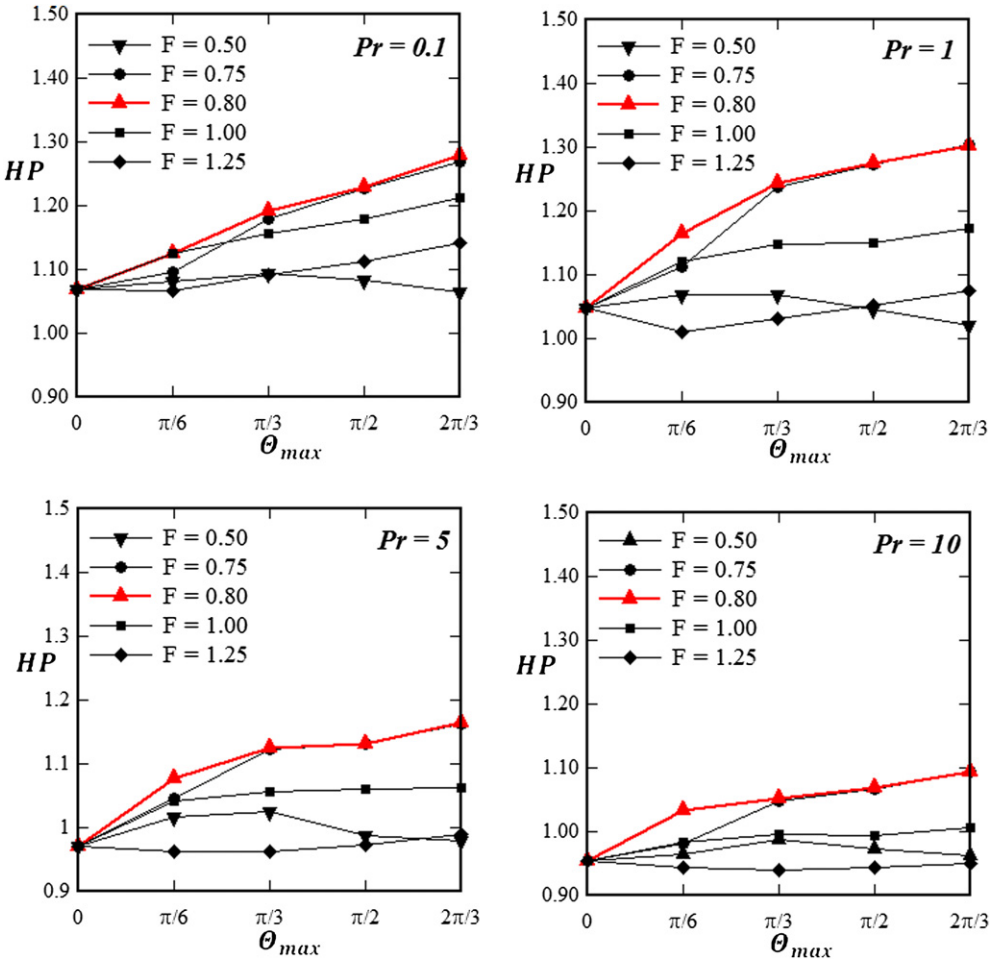

Fig. 9. Thermal effectiveness of the ROC design at different frequencies and amplitudes.

demonstrates variation of HP $= \overline{Nu}_{ave}/Nu_s^*$ versus amplitude for different fluids and excitation frequencies. HP values greater than 1 represent cases, where insertion of ROC is beneficial for channel cooling. From this figure a number of important conclusions can be drawn. First, for all cases examined, oscillation of the cylinder with frequency ratio of $F = 0.8$ provides the best cooling performance, and thus it is beneficial. Second, for all excitation frequencies, except $F = 0.5$, heat transfer performance improves with oscillation amplitude. Finally, heat transfer performance of oscillating cylinder is better for gases ($Pr<1$) than liquids ($Pr>1$).

4. Conclusions

Rotational oscillations of a cylinder confined in a channel are not affected by the limited gap between the cylinder and channel walls. Therefore, the ROC offers a wider oscillation amplitude range than the TOC cases, resulting in further heat transfer enhancement. Vortex dynamics, thermal boundary layer thickness and Prandtl number play important roles in heat transfer enhancement. A vortex shedding mechanism that can generate high intensity vortices and align them close to the channel walls is desirable. As a result, fluid rotation induced by the vortices interchanges hot and cold fluids near the wall and channel center after the formation region. Although increasing the excitation frequency generates higher vorticity magnitudes, the vortices start to form further away from the walls for $F \geq 0.85$, which reduces their effect on heat transfer. On the other hand, increasing the oscillation angle Θ_{max} enhances heat transfer continuously. Performance analysis compared to heat convection from a straight channel shows that all $F = 0.8$ cases provide better cooling performance than the other excitation frequencies; and $\Theta_{max} = 2\pi/3$, which is the highest oscillation angle used here, gives the best results. Power based performance analysis for $F = 0.8$ and $\Theta_{max} = 2\pi/3$ case results in 30% higher channel averaged Nusselt number than the corresponding straight channel case for $Pr = 1$ fluid. Results show the feasibility of using rotationally oscillating cylindrical actuators with air flow for electronic chip cooling applications.

References

[1] R.L. Webb, E.R.G. Eckert, R.J. Goldstein, Heat transfer and friction in tubes with repeated-rib roughness, Int. J. Heat Mass Transfer 14 (1971) 601–617.
[2] B. Celik, U. Akdag, S. Gunes, A. Beskok, Flow past an oscillating circular cylinder in a channel with an upstream splitter plate, Phys. Fluids 20 (2008) 103603.
[3] B. Celik, A. Beskok, Mixing induced by a transversely oscillating circular cylinder in a straight channel, Phys. Fluids 21 (2009) 073601.
[4] B. Celik, M. Raisee, A. Beskok, Heat transfer enhancement in a slot channel via a transversely oscillating adiabatic circular cylinder, Int. J. Heat Mass Transfer 53 (2010) 626–634.
[5] K. Sreenivasan, A. Ramachandran, Effect of vibration on heat transfer from a horizontal cylinder to a normal air stream, Int. J. Heat Mass Transfer 3 (1961) 60–67.
[6] U.C. Saxena, A.D.K. Laird, Heat transfer from a cylinder oscillating in a cross flow, J. Heat Transfer-Trans ASME 100 (1978) 684–689.
[7] C. Gau, J.M. Wu, C.Y. Liang, Heat transfer enhancement and vortex flow structure over a heated cylinder oscillating in the cross flow direction, J. Heat Transfer-Trans ASME 121 (1999) 789–795.

[8] S.J. Yang, Numerical study of heat transfer enhancement in a channel flow using an oscillating vortex generator, Heat and Mass Transfer 39 (2003) 257–265.
[9] W.S. Fu, B.H. Tong, Numerical investigation of heat transfer from a heated oscillating cylinder in a cross flow, Int. J. Heat Mass Transfer 45 (2002) 3033–3043.
[10] A. Okajima, H. Takata, T. Asanuma, Viscous Flow Around a Rotationally Oscillating Circular Cylinder University of Tokyo Report no. 5323, Institute of Space and Aeronautical Science, September 1975.
[11] S. Taneda, Visual observations of the flow past a sphere at Reynolds numbers between 10^4 and 10^6, J. Fluid Mech. 85 (1978) 187.
[12] J. Wu, J. Mo and A. Vakili, On the wake of a cylinder with rotational oscillations, AIAA 2nd Shear Flow Conference, March 13–16, 1989 Tempe, AZ.
[13] F.M. Mahfouz, H.M. Badr, Forced convection from a rotationally oscillating cylinder placed in a uniform stream, Int. J. Heat Mass Transfer 43 (2000) 3093–3104.
[14] S.J. Lee, J.Y. Lee, Flow structure of wake behind a rotationally oscillating circular cylinder, J. Fluids Structures 22 (2006) 1097–1112.
[15] G.E. Karniadakis, M. Israeli, S.A. Orszag, High-order splitting methods for the incompressible Navier Stokes equations, J. Computational Phys. 97 (1991) 414–443.
[16] G.E. Karniadakis, S.J. Sherwin, Spectral/hp Element Methods for CFD, Oxford University Press, Oxford UK, 2005.
[17] A. Beskok, T.C. Warburton, An unstructured hp finite-element scheme for fluid flow and heat transfer in moving domains, J. Computational Phys. 174 (2001) 492–509.
[18] W.S. Fu, B.H. Tong, Numerical investigation of heat transfer characteristics of the heated blocks in the channel with a transversely oscillating cylinder, Int. J. Heat Mass Transfer 47 (2004) 341–351.
[19] F.P. Incropera, D.P. Dewitt, Fundamentals of Head and Mass Transfer, John Wiley & Sons, New York, 2006.
[20] I.G. Currie, Fundamental Mechanics of Fluids, Marcel Dekker, New York, 2003, pp. 254–257.